

NuSTAR AND *XMM-NEWTON* OBSERVATIONS OF LUMINOUS, HEAVILY OBSCURED, *WISE*-SELECTED QUASARS AT $z \sim 2$

D. STERN¹, G. B. LANSBURY², R. J. ASSEF³, W. N. BRANDT^{4,5}, D. M. ALEXANDER², D. R. BALLANTYNE⁶, M. BALOKOVIĆ⁷,
F. E. BAUER^{8,9,10}, D. BENFORD¹¹, A. BLAIN¹², S. E. BOGGS¹³, C. BRIDGE⁷, M. BRIGHTMAN¹⁴, F. E. CHRISTENSEN¹⁵, A. COMASTRI¹⁶,
W. W. CRAIG^{13,17}, A. DEL MORO², P. R. M. EISENHARDT¹, P. GANDHI², R. L. GRIFFITH⁴, C. J. HAILEY¹⁸, F. A. HARRISON⁷,
R. C. HICKOX¹⁹, T. H. JARRETT²⁰, M. KOSS²¹, S. LAKE²², S. M. LAMASSA²³, B. LUO^{4,5}, C.-W. TSAI¹, C. M. URRY²³, D. J. WALTON⁷,
E. L. WRIGHT²², J. WU²², L. YAN²⁴, AND W. W. ZHANG¹¹

¹ Jet Propulsion Laboratory, California Institute of Technology, 4800 Oak Grove Drive, Mail Stop 169-221, Pasadena, CA 91109, USA; daniel.k.stern@jpl.nasa.gov

² Department of Physics, University of Durham, South Road, Durham DH1 3LE, UK

³ Núcleo de Astronomía de la Facultad de Ingeniería, Universidad Diego Portales, Av. Ejército Libertador 441, Santiago, Chile

⁴ Department of Astronomy and Astrophysics, The Pennsylvania State University, 525 Davey Lab, University Park, PA 16802, USA

⁵ Institute for Gravitation and the Cosmos, The Pennsylvania State University, University Park, PA 16802, USA

⁶ Center for Relativistic Astrophysics, School of Physics, Georgia Institute of Technology, Atlanta, GA 30332, USA

⁷ Cahill Center for Astronomy and Astrophysics, California Institute of Technology, Pasadena, CA 91125, USA

⁸ Instituto de Astrofísica, Facultad de Física, Pontificia Universidad Católica de Chile, 306, Santiago 22, Chile

⁹ Millennium Institute of Astrophysics, Vicuña Mackenna 4860, 7820436 Macul, Santiago, Chile

¹⁰ Space Science Institute, 4750 Walnut Street, Suite 205, Boulder, CO 80301, USA

¹¹ NASA Goddard Space Flight Center, Greenbelt, MD 20771, USA

¹² Physics & Astronomy, University of Leicester, 1 University Road, Leicester, LE1 7RH, UK

¹³ Space Sciences Laboratory, University of California, Berkeley, 7 Gauss Way, Berkeley, CA 94720-7450, USA

¹⁴ Max-Planck-Institut für extraterrestrische Physik, Giessenbachstrasse 1, D-85748, Garching bei München, Germany

¹⁵ Danish Technical University, DK-2800 Lyngby, Denmark

¹⁶ INAF Osservatorio Astronomico di Bologna, via Ranzani 1, I-40127, Bologna, Italy

¹⁷ Lawrence Livermore National Laboratory, Livermore, CA 94550, USA

¹⁸ Columbia Astrophysics Laboratory, Columbia University, New York, NY 10027, USA

¹⁹ Department of Physics and Astronomy, Dartmouth College, 6127 Wilder Laboratory, Hanover, NH 03755, USA

²⁰ Astrophysics, Cosmology and Gravity Centre, Department of Astronomy, University of Cape Town, Rondebosch, South Africa

²¹ Institute for Astronomy, Department of Physics, ETH Zurich, Wolfgang-Pauli-Strasse 27, CH-8093 Zurich, Switzerland

²² Division of Astronomy & Astrophysics, University of California, Los Angeles, Los Angeles, CA 90095-1547, USA

²³ Department of Physics and Yale Center for Astronomy and Astrophysics, Yale University, New Haven, CT 06520-8120, USA

²⁴ Infrared Processing and Analysis Center, Department of Astronomy, California Institute of Technology, Pasadena, CA 91125, USA

Received 2014 March 21; accepted 2014 July 23; published 2014 September 29

ABSTRACT

We report on a *NuSTAR* and *XMM-Newton* program that has observed a sample of three extremely luminous, heavily obscured *WISE*-selected active galactic nuclei (AGNs) at $z \sim 2$ across a broad X-ray band (0.1 – 79 keV). The parent sample, selected to be faint or undetected in the *WISE* 3.4 μm (*W1*) and 4.6 μm (*W2*) bands but bright at 12 μm (*W3*) and 22 μm (*W4*), are extremely rare, with only ~ 1000 so-called “*W1W2*-dropouts” across the extragalactic sky. Optical spectroscopy reveals typical redshifts of $z \sim 2$ for this population, implying rest-frame mid-IR luminosities of $\nu L_{\nu}(6 \mu\text{m}) \sim 6 \times 10^{46} \text{ erg s}^{-1}$ and bolometric luminosities that can exceed $L_{\text{bol}} \sim 10^{14} L_{\odot}$. The corresponding intrinsic, unobscured hard X-ray luminosities are $L(2\text{--}10 \text{ keV}) \sim 4 \times 10^{45} \text{ erg s}^{-1}$ for typical quasar templates. These are among the most AGNs known, though the optical spectra rarely show evidence of a broad-line region and the selection criteria imply heavy obscuration even at rest-frame 1.5 μm . We designed our X-ray observations to obtain robust detections for gas column densities $N_{\text{H}} \leq 10^{24} \text{ cm}^{-2}$. In fact, the sources prove to be fainter than these predictions. Two of the sources were observed by both *NuSTAR* and *XMM-Newton*, with neither being detected by *NuSTAR* ($f_{3\text{--}24 \text{ keV}} \lesssim 10^{-13} \text{ erg cm}^{-2} \text{ s}^{-1}$), and one being faintly detected by *XMM-Newton* ($f_{0.5\text{--}10 \text{ keV}} \sim 5 \times 10^{-15} \text{ erg cm}^{-2} \text{ s}^{-1}$). A third source was observed only with *XMM-Newton*, yielding a faint detection ($f_{0.5\text{--}10 \text{ keV}} \sim 7 \times 10^{-15} \text{ erg cm}^{-2} \text{ s}^{-1}$). The X-ray data imply these sources are either X-ray weak, or are heavily obscured by column densities $N_{\text{H}} \gtrsim 10^{24} \text{ cm}^{-2}$. The combined X-ray and mid-IR analysis seems to favor this second possibility, implying the sources are extremely obscured, consistent with Compton-thick, luminous quasars. The discovery of a significant population of heavily obscured, extremely luminous AGNs would not conform to the standard paradigm of a receding torus, in which more luminous quasars are less likely to be obscured, and instead suggests that an additional source of obscuration is present in these extreme sources.

Key words: galaxies: active – quasars: individual (WISEA J181417.29+341224.8, WISEA J220743.82+193940.1, WISEA J235710.82+032802)

Online-only material: color figures

1. INTRODUCTION

The *Wide-field Infrared Survey Explorer* (*WISE*; Wright et al. 2010) is an extremely capable and efficient black hole finder. As demonstrated in selected fields by *Spitzer* (e.g., Stern et al.

2005; Donley et al. 2012), the same material that obscures active galactic nuclei (AGNs) at UV, optical, and soft X-ray energies is heated by the AGN and emits strongly at mid-IR wavelengths. The all-sky *WISE* survey identifies millions of obscured and unobscured quasars across the full sky (e.g., Stern et al. 2012;

Assef et al. 2013), as well as very rare populations of extremely luminous, heavily obscured AGNs.

In terms of the latter, the *WISE* extragalactic team has been pursuing sources that are faint or undetected in *WISE* W1 ($3.4\ \mu\text{m}$) and W2 ($4.6\ \mu\text{m}$), but are bright in W3 ($12\ \mu\text{m}$) and W4 ($22\ \mu\text{m}$). We refer to this population as W1W2-dropouts (Eisenhardt et al. 2012). This is a very rare population; selecting to a depth of 1 mJy at $12\ \mu\text{m}$, there are only ~ 1000 such sources across the extragalactic sky (~ 1 per $30\ \text{deg}^2$). These objects are undetected by *ROSAT* and tend to be optically faint ($r \gtrsim 23$), below the detection threshold of Sloan Digital Sky Survey (SDSS). We have obtained spectroscopic redshifts for >100 W1W2-dropouts thus far, consistently finding redshifts $z \gtrsim 2$, with our current highest redshift source at $z = 4.6$ (P. R. Eisenhardt et al. 2014, in preparation). Approximately half of the sources show clear type-2 AGN signatures in the optical spectra, with the other half typically showing only Ly α emission, sometimes extended, which could be due to star formation and/or AGN activity (Bridge et al. 2013). The lack of a far-IR peak in their broadband spectral energy distributions (SEDs) suggests the dominant energy input for this population comes from a heavily obscured AGN and not extreme starbursts (e.g., Eisenhardt et al. 2012; Wu et al. 2012). Related high-luminosity sources selected from the *WISE* satellite have also recently been reported by Weedman et al. (2012) and Alexandroff et al. (2013), while several teams have identified less rare, less luminous sources from *Spitzer* surveys (e.g., Dey et al. 2008; Fiore et al. 2009; Lanzuisi et al. 2009). Considering just one of these latter samples in more detail for comparison, Lanzuisi et al. (2009) study a sample of mid-IR-selected obscured AGNs in the Spitzer Wide-area Infra-Red Extragalactic survey (Lonsdale et al. 2003). Selecting bright mid-IR sources ($f_{24\ \mu\text{m}} > 1.3\ \text{mJy}$) with extreme mid-IR to optical flux ratios ($f_{24\ \mu\text{m}}/f_R > 2000$), they find 44 sources within $6\ \text{deg}^2$. Follow-up shows typical redshifts of $0.7 \lesssim z \lesssim 2.5$. This implies mid-IR luminosities a factor of $\sim 30\times$ lower than the W1W2-dropout population, with a surface density $>200\times$ higher.

Here we report on the first targeted X-ray follow-up of the extreme W1W2-dropout population. We observed two sources with both the *Nuclear Spectroscopic Telescope Array* (*NuSTAR*; Harrison et al. 2013) and *XMM-Newton* (Jansen et al. 2001); a third source was only observed by *XMM-Newton*. Unless otherwise specified, we use Vega magnitudes throughout and adopt the concordance cosmology, $\Omega_M = 0.3$, $\Omega_\Lambda = 0.7$ and $H_0 = 70\ \text{km s}^{-1}\ \text{Mpc}^{-1}$.

2. SAMPLE

Figure 1 presents the optical spectra of the three W1W2-dropouts targeted for X-ray follow-up: WISEA J181417.29+341224.8 (hereafter, WISE J1814+3412), WISEA J220743.82+193940.1 (hereafter, WISE J2207+1939), and WISEA J235710.82+032802.8 (hereafter, WISE J2357+0328). The spectra were all obtained with the Low Resolution Imaging Spectrometer (LRIS; Oke et al. 1995) on the Keck I telescope, between 2010 July and 2010 November. The sources were selected on the basis of having unusually red colors across the *WISE* passbands in the initial All-Sky *WISE* data release: $W1 > 17.4$, $W4 < 7.7$, and $W2 - W4 > 8.2$ (for further details on the W1W2-dropout selection, see Eisenhardt et al. 2012). The most likely interpretation of sources with these extreme colors is that they host an extremely luminous, heavily obscured AGN which only becomes evident at observed wavelengths $\gtrsim 10\ \mu\text{m}$. The W1 flux limit essentially

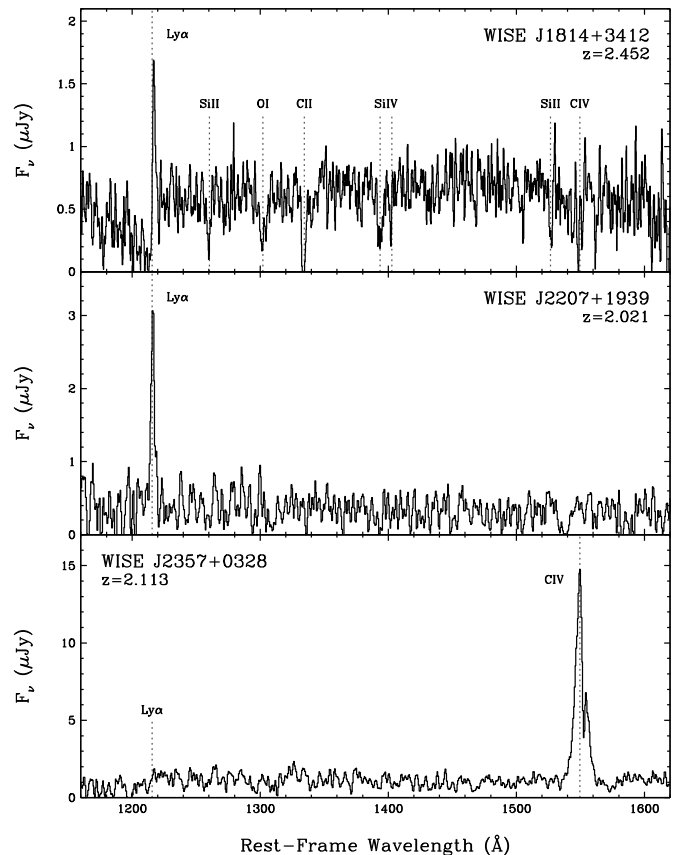


Figure 1. Keck/LRIS spectra of the three extreme *WISE*-selected obscured AGNs at $z \sim 2$ which we observed at X-ray energies.

constrains the sample to $z \gtrsim 1.5$ for the host galaxy not to be detected.

Note the diversity of the optical spectra of the three sources targeted for X-ray follow-up (Figure 1). This is representative of the diverse optical spectroscopic properties of the W1W2-dropout population in general (Wu et al. 2012; P. R. Eisenhardt et al. 2014, in preparation). Eisenhardt et al. (2012) discusses WISE J1814+3412 in depth: briefly, the optical spectrum is indistinguishable from an L^* Lyman-break galaxy (LBG) at $z \sim 2.5$ (e.g., Shapley et al. 2003), with no obvious signature of a (buried) AGN. However, typical LBGs have $22\ \mu\text{m}$ flux densities a factor of 1000 lower (Reddy et al. 2006). The redshift of WISE J2207+1939 is based on a single, asymmetric, high equivalent width emission line which is reliably identified as Ly α $\lambda 1216$ (for a detailed discussion of one-line redshifts, see Stern et al. 2000). WISE J2357+0328 shows a high equivalent width ($\sim 300\ \text{\AA}$, observed), slightly broadened (FWHM $\sim 1500\ \text{km s}^{-1}$), self-absorbed line identified as C IV $\lambda 1549$, which is a common strong line in AGNs. However, quite unusually, no Ly α emission is evident. The only strong feature blue-ward of the emission line is a continuum break at observed $\sim 3785\ \text{\AA}$, which is consistent with the Ly α forest break for the longer wavelength emission line being C IV. Hall et al. (2004) reports on a detailed investigation of a similar SDSS quasar with broad C IV emission, but lacking broad Ly α emission. They argue that the unusual spectrum cannot be solely due to dust extinction in the broad-line region (BLR), and instead suggest that most, but not all, of the spectral properties can be explained by an unusually high density gas in the BLR ($n_H \sim 10^{15}\ \text{cm}^{-3}$) with an incident power-law continuum extending to $\geq 200\ \mu\text{m}$. Clearly the unusual optical spectrum of WISE J2357+0328 is

Table 1
Source Properties

	WISE J1814+3412	WISE J2207+1939	WISE J2357+0328
R.A. (J2000)	18:14:17.29	22:07:43.82	23:57:10.82
Decl. (J2000)	+34:12:24.8	+19:39:40.1	+03:28:02.8
z	2.452	2.021	2.113
$W1$ ($3.4 \mu\text{m}$)	18.861 ± 0.440	17.174 ± 0.127	>18.142
$W2$ ($4.6 \mu\text{m}$)	17.609 ± 0.492	16.136 ± 0.170	>16.614
$W3$ ($12 \mu\text{m}$)	10.410 ± 0.061	10.630 ± 0.106	10.088 ± 0.068
$W4$ ($22 \mu\text{m}$)	6.863 ± 0.071	7.135 ± 0.101	6.942 ± 0.112
(3.6)	17.707 ± 0.023	17.023 ± 0.048	17.487 ± 0.076
(4.5)	17.021 ± 0.020	16.208 ± 0.025	16.544 ± 0.036
$S_{1.4 \text{ GHz}}$	~ 1.4	5.2 ± 0.4	<0.8
$f_{0.5-2 \text{ keV}}$	0.109 ± 0.053	<0.264	<0.243
$f_{2-10 \text{ keV}}$	<1.30	<0.780	1.05 ± 0.53
$f_{0.5-10 \text{ keV}}$	0.521 ± 0.141	<0.523	0.73 ± 0.31
$f_{3-24 \text{ keV}}$	<7.55	<6.04	...
$L_{6 \mu\text{m}}$	20.10 ± 2.40	8.28 ± 1.62	5.04 ± 0.36
$E(B - V)_{\text{AGN}}$	15.1 ± 1.1	17.6 ± 2.3	5.5 ± 0.4
$L_{2-10 \text{ keV}}$	1.04	<1.13	<1.14
$L_{10-40 \text{ keV}}$	<17.1	<10.1	...

Notes. Astrometry and *WISE* photometry are from the AllWISE release; mid-IR photometry is all in Vega magnitudes and *WISE* limits report the 95% confidence lower limit to the apparent magnitude. *Spitzer* photometry, in brackets, is from Griffith et al. (2012). Radio flux densities are in units of mJy; see the text in the final paragraph of Section 2 for details. The radio non-detection corresponds to the typical 5σ depth of FIRST. X-ray fluxes, all in the observed frame, are in units of $10^{-14} \text{ erg cm}^{-2} \text{ s}^{-1}$. $L_{6 \mu\text{m}}$ is the rest-frame $6 \mu\text{m}$ luminosity (νL_ν) of the AGN in units of $10^{46} \text{ erg s}^{-1}$. Rest-frame X-ray luminosities are in units of $10^{44} \text{ erg s}^{-1}$. We report 68% confidence limit (CL) uncertainties on the X-ray fluxes; upper limits correspond to the 90% CL.

worthy of future study, but such analysis is beyond the scope of the current paper which focuses on the X-ray properties of the *W1W2*-dropout population.

Table 1 presents basic source properties and multi-wavelength photometry for the three X-ray-targeted *W1W2*-dropouts. We list mid-IR data from the AllWISE data release²⁵ and *Spitzer*, where the latter comes from the *Warm Spitzer* observations reported by Griffith et al. (2012). Comparing the AGN luminosity and reddening of WISE J1814+3412 derived solely from the mid-IR photometry (Section 4.1) to the values in Eisenhardt et al. (2012) derived from 16-band multi-wavelength photometry, we obtain consistent values within $\sim 10\%$.

In terms of their radio properties, WISE J1814+3412 has a counterpart offset by $6''.1$ in the NRAO/VLA Sky Survey (NVSS; Condon et al. 1998) with a flux density $S_{1.4 \text{ GHz}} = 3.4 \pm 0.5 \text{ mJy}$. Eisenhardt et al. (2012) report on follow-up radio observations of this source with the Jansky Very Large Array (VLA) at 4.94 GHz and 7.93 GHz. These data clearly resolve the NVSS emission into two distinct sources, the fainter of which is associated with WISE J1814+3412; using the measured spectral index to extrapolate the *L*-band brightness of that source predicts a 1.4 GHz flux density of 1.4 mJy. Based on both its rest-frame 1.4 GHz radio luminosity ($L_{1.4 \text{ GHz}} \sim 5 \times 10^{25} \text{ W Hz}^{-1}$) and its radio-to-optical ratio (rest-frame $L_{5 \text{ GHz}}/L_{0.44 \mu\text{m}} \sim 200$), WISE J1814+3412 qualifies as radio-loud. WISE J2207+1939 has a counterpart offset by $7''.1$ in the NVSS with $S_{1.4 \text{ GHz}} = 5.2 \pm 0.4 \text{ mJy}$, suggesting that it is also radio loud. WISE J2357+0328 has no radio counterpart in either NVSS or the VLA Faint Images of the Radio Sky at Twenty Centimeters

survey (FIRST; Becker et al. 1995). The radio luminosities of the first two sources further indicate the presence of a powerful AGN in this *WISE*-selected population.

3. X-RAY OBSERVATIONS

3.1. *NuSTAR* Observations

In 2012 October *NuSTAR* obtained ~ 20 ks observations of WISE J1814+3412 and WISE J2207+1939; details of the observations, including net exposure times, are provided in Table 2. We processed the level 1 data using the *NuSTAR* Data Analysis Software (NuSTARDAS) v.1.2.0, and produced calibrated and cleaned event files (level 2 data) for both *NuSTAR* focal plane modules (FPMA and FPMB) using *nupipeline* and the most current available version of the Calibration Database files (CALDB 20130509).

Neither source was detected, though a serendipitous broad-lined AGN at $z = 0.763$ was identified in the WISE J1814+3412 field (Alexander et al. 2013). We measured gross source counts in $45''$ radius apertures centered on the *WISE* positions and local background counts from an annulus of inner radius $90''$ and outer radius $150''$ centered on the sources. We performed photometry in the observed-frame 3–24 keV, 3–8 keV and 8–24 keV bands, as well as the rest-frame 10–40 keV band for both FPMs and used binomial statistics to determine the likelihood of the sources being detected. Binomial statistics are more accurate than Poisson statistics at these faint limits since it takes into account uncertainty in the measured background (i.e., it takes the total background counts into account, not just the scaled background counts). We use binomial statistics to calculate the probability that the measured source counts are purely due to background fluctuations (i.e., false, or ‘no-source’ probabilities; for details, see Lansbury et al. 2014). For both *WISE* sources the probability of a false *NuSTAR* detection based on the binomial statistics is $>15\%$. As we take a no-source probability $<1\%$ to indicate a detection, neither source was detected. Since binomial statistics are not amenable to plotting simple tracks, Figure 2 shows the X-ray counts with Poisson no-source probabilities. The latter provide a good approximation of binomial probabilities for our sources given the reasonably high background count rates.

Table 1 reports the 90% confidence limit upper limits to the flux in the 3–24 keV energy band, calculated using the Bayesian method of Kraft et al. (1991). To convert count rate to source flux, we used XSPEC v12.8.0k, taking into account the Response Matrix File (RMF) and Ancillary Response File (ARF) for each FPM. We assumed a power-law model with $\Gamma = 1.8$. Assuming a harder intrinsic spectrum does not qualitatively change these results; e.g., adopting $\Gamma = 1.0$ only changes the rest-frame 10–40 keV luminosities by $\leq 3\%$.

3.2. *XMM-Newton* Observations

We obtained ~ 30 ks observations of the three *W1W2*-dropouts between 2012 October and 2013 January with the *XMM-Newton* EPIC-MOS (Turner et al. 2001) and EPIC-pn (Strüder et al. 2001) cameras. Details of the observations are provided in Table 2. We used data products from the Pipeline Processing System (PPS), analyzed with the Science Analysis Software²⁶ (SAS v.12.0.1). Good time intervals were identified by PPS, eliminating $\sim 1\%$ of the exposure time for the MOS cameras and $\sim 10\%$ of the exposure times for EPIC-pn. We then

²⁵ <http://wise2.ipac.caltech.edu/docs/release/allwise/>

²⁶ <http://xmm.esa.int/sas/>

Table 2
X-Ray Observation Log

Target Name	z	<i>NuSTAR</i>			<i>XMM-Newton</i>		
		Observation ID	UT Date	Exposure (ks)	Observation ID	UT Date	MOS1/MOS2/pn Exposure (ks)
(1)	(2)	(3)	(4)	(5)	(6)	(7)	(8)
WISE J1814+3412	2.452	60001114002	2012 Oct 30	21.3	0693750101	2012 Oct 07	29.6/29.6/19.6
WISE J2207+1939	2.021	60001115002	2012 Oct 30	20.8	0693750201	2012 Nov 22	18.4/18.7/11.5
WISE J2357+0328	2.113	0693750401	2013 Jan 02	29.1/28.7/14.4

Notes. (1) Target name; full name and coordinates are in Table 1. (2) Redshift. (3) and (4) *NuSTAR* observation ID and start date. (5) Net on-axis *NuSTAR* exposure time. This value applies for both FPMA and FPMB. The target was on-axis for both of the *NuSTAR* observations. (6) and (7) *XMM-Newton* observation ID and start date. (8) Net on-axis exposure time, corrected for flaring and bad events, for the MOS cameras and the pn camera, as indicated.

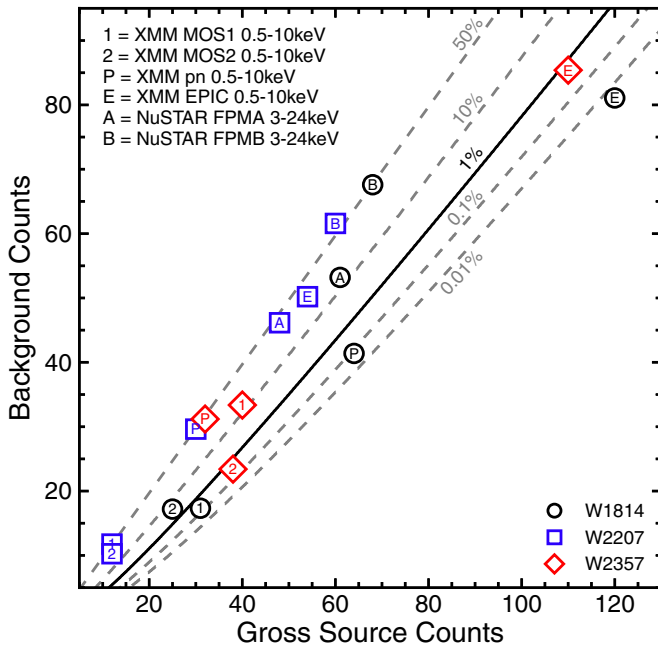


Figure 2. Gross source counts vs. background counts (scaled to the source region) for WISE J1814+3412, WISE J2207+1939, and WISE J2357+0328 (circles, squares, and diamonds, respectively). The 1, 2, and p labels correspond to the 0.5–10 keV counts for the EPIC-MOS1, EPIC-MOS2, and EPIC-pn cameras on *XMM-Newton*, respectively, while the E labels correspond to merging the photons from the three EPIC cameras together. The A and B labels correspond to the 3–24 keV counts for FPMA and FPMB on *NuSTAR*, respectively. The dashed lines indicate Poisson no-source probabilities. Two sources are faintly detected: WISE J1814+3412 is detected with the EPIC-MOS1 and EPIC-pn cameras, and WISE J2357+0328 is detected with the EPIC-MOS2 camera.

(A color version of this figure is available in the online journal.)

identified flares using SAS, resulting in the effective exposure times listed in Table 2. We measured 0.5–10 keV source counts in 15'' radius apertures centered on the *WISE* positions. For most observations, we measured local backgrounds in slightly offset source-free circular apertures with radii of $\sim 70''$ – $100''$ selected to avoid serendipitous sources and chip gaps. The exceptions were the EPIC-MOS observations of WISE J2357+0328 which had no nearby serendipitous sources and thus allowed for a $30''$ – $70''$ radius annulus centered the source position.

As above with the *NuSTAR* observations, we calculated binomial false probabilities and plot the equivalent using Poisson statistics in Figure 2. Only WISE J1814+3412 is reliably detected, with a binomial no-source probability of 0.04% with EPIC-pn and 0.1% with EPIC-MOS1; WISE J1814+3412 was not reliably detected with EPIC-MOS2. WISE J2357+0328 is weakly detected with EPIC-MOS2 with a no-source probability

of 0.2%, and is undetected with the other two cameras. Figure 2 also shows the binomial false probabilities for the photons from the three EPIC cameras merged together, which produces essentially identical results. We find a slightly stronger detection of WISE J1814+3412, a similar significance detection of WISE J2357+0328 (still detected with a false probability of $\sim 0.2\%$), and WISE J2207+1939 remains undetected.

We used XSPEC to convert count rate (or count rate limits) to flux, assuming a power-law model with $\Gamma = 1.8$, and the *XMM-Newton* RMFs and ARFs for each EPIC camera. Again, adopting a harder intrinsic X-ray spectrum would have a modest quantitative effect on the derived luminosities, but would not affect our broad conclusions. Specifically, were we to instead assume $\Gamma = 1.0$, the rest-frame 2–10 keV luminosities would change by $\leq 18\%$.

Finally, we note that the relatively large difference between the EPIC-pn and EPIC-MOS net exposure times in Table 2 are due to significant flaring events identified by the SAS task `tabgtigen` in the former data. The tabulated numbers are for a conservative threshold of $RATE > 0.4$ for EPIC-pn, though we have verified that the source detection results are essentially unchanged for a more liberal threshold of $RATE > 1.0$.

4. RESULTS

4.1. AGN Properties from Mid-IR Data

We modeled the SED of each source using the Assef et al. (2010) 0.03–30 μm empirical AGN and galaxy templates. Figure 3 presents the fitting results for WISE J2207+1939 and WISE J2357+0328; a similar plot of the broadband SED of WISE J1814+3412 is presented in Eisenhardt et al. (2012). Each SED is modeled as a best-fit, non-negative combination of an elliptical, spiral, and irregular galaxy component, plus an AGN component. Only the AGN component is fit for dust reddening (for further details on the SED models, see Assef et al. 2008, 2010). The modeling outputs $L_{6\mu\text{m}}$, the derived intrinsic luminosity (νL_ν) of the AGN component at rest-frame 6 μm , as well as the reddening of the AGN component, $E(B - V)_{\text{AGN}}$ (see Table 1). For the typical gas to dust ratio observed by Maiolino et al. (2001) for luminous AGNs ($L_X \gtrsim 10^{42} \text{ erg cm}^{-2} \text{ s}^{-1}$), the nuclear reddening values of $E(B - V)_{\text{AGN}} \sim 5$ – 20 suggests gas columns of $N_{\text{H}} \sim (5$ – $20) \times 10^{23} \text{ cm}^{-2}$, which reach into the Compton-thick regime ($N_{\text{H}} \geq 1.5 \times 10^{24} \text{ cm}^{-2}$). However, we note that this extrapolates the work of Maiolino et al. (2001) to higher AGN luminosities as well as to narrow-lined AGNs. Furthermore, the Maiolino et al. (2001) sample hints at a 0.5 dex shift in the gas to dust ratio for more luminous AGNs, albeit based on just five sources with $L_X > 10^{43.5} \text{ erg cm}^{-2} \text{ s}^{-1}$. The

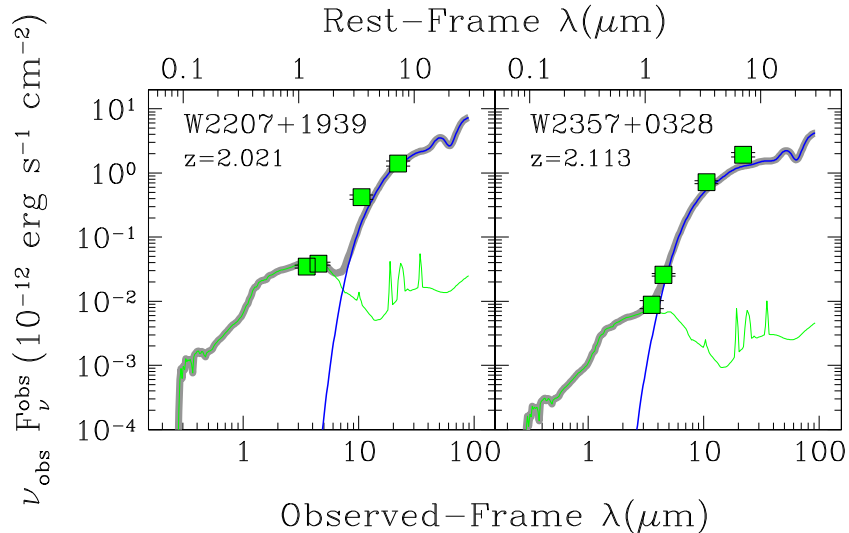


Figure 3. Best-fitting SED template models (heavy gray line) to the *WISE* photometry (shown by green symbols) for WISE J2207+1939 and WISE J2357+0328. The fits use the Sbc spiral (green) and type-1 AGN (blue) empirical templates from Assef et al. (2010), with the amount of reddening for the AGN component a free parameter. The host galaxy dominates at observed $\lambda \lesssim 5 \mu\text{m}$, while the heavily obscured AGN dominates at longer wavelengths. Note that the best-fit models shown here find the stellar light dominated by the spiral template, while the modeling (and associated uncertainties listed in Table 1) use all three galaxy templates from Assef et al. (2010; see Section 4.1).

(A color version of this figure is available in the online journal.)

direction of this shift is such that less X-ray absorbing gas is required for a given dust column for the most luminous AGNs.

4.2. Indirect X-Ray Absorption Constraints

The mid-IR properties of *W1W2*-dropouts indicate the presence of extremely luminous, heavily obscured AGNs, with bolometric luminosities approaching, or even exceeding $L_{\text{bol}} \sim 10^{14} L_{\odot}$ (Eisenhardt et al. 2012; Wu et al. 2012; Bridge et al. 2013; Assef et al. 2014; Jones et al. 2014; C. Tsai et al. 2014, in preparation). Given the heavy obscuration implied by their mid-IR SEDs and optical spectra, it is perhaps unsurprising that the three sources we targeted for X-ray follow-up are either undetected or only faintly detected, despite observing at the penetrating energies above rest-frame 10 keV which are less affected by absorption. But what are their absorption column densities? We can obtain indirect estimates of this from their mid-IR luminosities since unobscured AGNs tend to have a fairly tight relation between their mid-IR and X-ray luminosities.

Figure 4 compares the rest-frame $6 \mu\text{m}$ and X-ray luminosities for our targeted sources. We show published relations from Lutz et al. (2004), Gandhi et al. (2009) and Fiore et al. (2009); the relation of Lanzuisi et al. (2009) is very similar to that of Fiore et al. (2009) for $L_{6\mu\text{m}} \geq 10^{45} \text{ erg s}^{-1}$. We plot non-beamed AGNs with $L_X > 10^{43} \text{ erg s}^{-1}$ from the *NuSTAR* serendipitous survey (Alexander et al. 2013); the serendipitous sources all lie within the scatter of the published relations. We also show Compton-thick quasars observed at soft energies from Alexander et al. (2008), three SDSS type-2 quasars observed by *NuSTAR* (Lansbury et al. 2014), and an obscured quasar at $z \approx 2$ detected by *NuSTAR* in the Extended Chandra Deep Field South (ECDFS; Del Moro et al. 2014). The literature obscured AGN and the *WISE*-selected *W1W2*-dropouts generally lie significantly below the published relations. Assuming the suppression of their X-ray emission is due to absorption rather than intrinsic X-ray weakness, we can estimate their column densities from the dashed lines in Figure 4, which apply columns of $N_{\text{H}} = 10^{24} \text{ cm}^{-2}$ to the published relations. These were calculated using the MYTorus model (Murphy & Yaqoob

2009) with photon index $\Gamma = 1.8$ and a torus inclination angle $\theta_{\text{obs}} = 70^\circ$. The implication is that all three targeted sources are obscured, possibly heavily obscured or Compton-thick. For the rest-frame 2–10 keV panel, the one detected source, WISE J1814+3412, has a column of $N_{\text{H}} \sim 10^{24} \text{ cm}^{-2}$ for the Fiore et al. (2009) relation, and yet higher columns for the other two relations. The undetected sources require minimum columns of $N_{\text{H}} \sim 10^{24} \text{ cm}^{-2}$ for all but the Fiore et al. (2009) relation. Constraints from the *NuSTAR* nondetections are less strict, but are again consistent with heavy absorption columns. Furthermore, two of the three *WISE*-selected targets are radio-loud. Since optically selected radio-loud quasars tend to have extra X-ray emission as compared to radio-quiet quasars (Miller et al. 2011), this suggests yet larger minimum absorption columns for WISE J1814+3412 and WISE J2207+1939. In addition, the jet-linked X-ray emission is apparently subject to similarly high obscuration as the nuclear X-ray emission.

5. DISCUSSION

We designed our X-ray integration times to provide robust detections for (1) typical intrinsic AGN SEDs, and (2) gas column densities $N_{\text{H}} \lesssim 10^{24} \text{ cm}^{-2}$. None of the three sources were strongly detected, implying that at least one of the assumptions in our experimental design does not hold.

NuSTAR has now observed a range of obscured AGNs, from famous, local sources such as Mrk 231 (Teng et al. 2014), Circinus (Arévalo et al. 2014), NGC 424 (Baloković et al. 2014), and NGC 4945 (Puccetti et al. 2014), to higher redshift obscured quasars at $z \sim 0.5$ from SDSS (Lansbury et al. 2014) and $z \sim 2$ in the ECDFS (Del Moro et al. 2014). A recurring theme of these observations is that several AGNs which are extremely luminous at certain wavelengths, such as in the mid-IR or [O III] $\lambda 5007$, remain faint at X-ray energies. For some objects, this is the case even for the more penetrating hard X-rays $> 10 \text{ keV}$. For some sources, such as optically bright ($B \lesssim 16$) broad-absorption line (BAL) quasars from the Palomar-Green (PG) survey (Schmidt & Green 1983) and Mrk 231, we consider, and sometimes even favor attributing the hard X-ray faintness

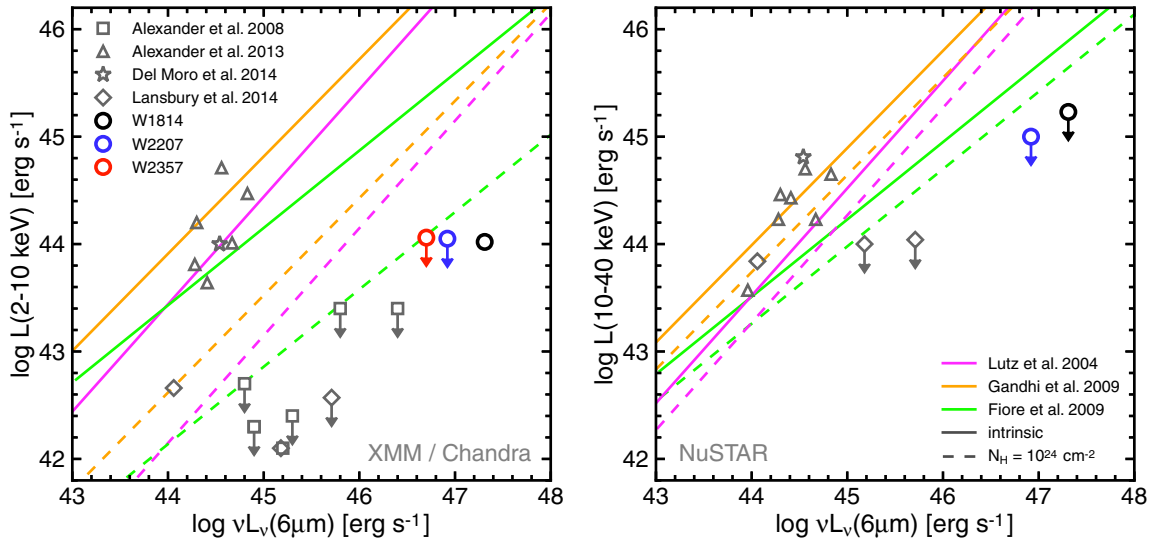


Figure 4. Rest-frame X-ray luminosity against rest-frame $6\mu\text{m}$ luminosity for: (left) 2–10 keV luminosities calculated using *XMM-Newton* data; and (right) 10–40 keV luminosities calculated using *NuSTAR* data. The X-ray luminosities are not corrected for absorption, and upper limits correspond to 3σ values to aid literature comparisons. WISE J1814+3412, WISE J2207+1939, and WISE J2357+0328 are shown as black, blue, and red circles, as indicated. We compare with *NuSTAR* observations from the serendipitous survey (Alexander et al. 2013; triangles), a survey of three SDSS type-2 quasars at $z \sim 0.5$ (Lansbury et al. 2014; diamonds), and an interesting source at $z \approx 2$ detected by *NuSTAR* in the ECDFS (Del Moro et al. 2014; star); in the left panel, we also show soft X-ray data on Compton-thick quasars from Alexander et al. (2008; squares). We compare with three published intrinsic relations for the 2–10 keV band calibrated using various AGN samples, as indicated. The relations are extrapolated to the 10–40 keV band assuming $\Gamma = 1.8$ and in both panels the dashed lines show the result of obscuration by $N_{\text{H}} = 10^{24} \text{ cm}^{-2}$. Assuming the low X-ray luminosities are due to absorption, sources that lie below the $N_{\text{H}} = 10^{24} \text{ cm}^{-2}$ tracks may be Compton-thick. (A color version of this figure is available in the online journal.)

to intrinsic X-ray weakness (Luo et al. 2013, 2014; Teng et al. 2014). Such intrinsic X-ray weakness seems the most plausible scenario when the X-ray data are of sufficient quality to allow a detailed X-ray spectral analysis, and that analysis implies only a moderately obscured AGN with an intrinsic X-ray luminosity significantly below the intrinsic AGN luminosity inferred from other wavebands—particularly for sources with strong UV continuum and broad emission lines, such as BAL quasars. Intrinsic X-ray weakness could be an aspect of the “disk-wind” model of BAL systems, in which the BAL wind is launched from the AGN accretion disk close to the black hole and is radiatively driven by UV line pressure (e.g., Proga et al. 2000). An intrinsically X-ray weak AGN could explain why the central engine does not over-ionize the gas, thereby quenching the line-driving mechanism. For a more detailed description of the intrinsically X-ray weak scenario, see Luo et al. (2013, 2014) and Teng et al. (2014).

For the three *WISE*-selected AGNs discussed here we obviously do not have the X-ray data to allow the full X-ray spectral analysis that might confidently imply intrinsic X-ray weakness. However, these sources show neither strong UV continuum nor broad emission lines, and we therefore favor interpreting the X-ray faintness as being due to a typical AGN seen through extremely high absorbing columns. This interpretation is consistent with both their mid-IR SEDs and their broad-line-free optical spectra. Indeed, the X-ray column constraints from Figure 4 are broadly consistent with the mid-IR measurements given typical luminous AGN gas-to-dust ratios from Maiolino et al. (2001). What is more surprising is that these sources, among the most bolometrically luminous AGNs known, appear heavily obscured. Various observations have shown that more luminous AGNs are less likely to be obscured (e.g., Ueda et al. 2003; Simpson 2005; Assef et al. 2013). This is consistent with the “receding torus model,” first proposed by Lawrence (1991), in which the height of the torus is independent of luminosity while the inner radius of the torus, corresponding to

the distance at which dust reaches its sublimation temperature, increases with luminosity. Therefore, in this model, more luminous AGNs have more sightlines into the nucleus and thus have a lower likelihood of being obscured.

The *W1W2*-dropout population is a rare population, with a surface density of just one source per $\sim 30 \text{ deg}^2$ in the extragalactic sky. The mid-IR luminosities imply intrinsic X-ray luminosities of a few $\times 10^{45} \text{ erg s}^{-1}$ from the relations of Lutz et al. (2004) and Gandhi et al. (2009). Just et al. (2007) report on X-ray follow-up of the most luminous quasars in SDSS, finding 35 quasars across 4188 deg^2 , or one source per $\sim 120 \text{ deg}^2$. The X-ray luminosities of this luminous quasar sample prove comparable to the expected intrinsic X-ray luminosities from the *WISE*-selected sample, implying the surprising discovery of comparable numbers of obscured and unobscured quasars at the top of the luminosity function. Assef et al. (2014) and C. Tsai et al. (2014, in preparation) present more detailed comparisons between the *W1W2*-dropout and luminous unobscured quasar populations, finding similar results.

The discovery of a significant population of heavily obscured, extremely luminous AGNs does not conform to the simple receding torus model, suggesting an additional source of obscuration. Indeed, the models of Draper & Ballantyne (2010) predict that Compton-thick AGNs should be more common at higher redshift because of the high fueling rates of quasars require significant gas reservoirs. Observationally, several authors have demonstrated that the obscured AGN fraction increases with redshift (for a given AGN luminosity; e.g., see La Franca et al. 2005; Hasinger 2008; Ueda et al. 2014). This is consistent with models showing that mergers may be more prominent in fueling AGNs at $z \sim 2$ (e.g., Hopkins et al. 2006, 2008; Menci et al. 2006; Draper & Ballantyne 2012). Indeed, these models also predict that the unified model of AGNs will break down for high-luminosity AGNs at $z \gtrsim 1$ because the obscuration is not confined to the nucleus (see also Draper & Ballantyne 2011).

Further investigations into this interesting population are clearly warranted. Deeper X-ray observations, achieving robust detections rather than faint and non-detections, would be valuable. Based on the EPIC-pn count rate ($0.78 \text{ counts ks}^{-1}$), we predict that it would require a $\sim 500 \text{ ks}$ *NuSTAR* observation of WISE J1814+3412 to achieve a robust detection in the 8–24 keV band (Poisson false probability $\leq 1\%$) for $N_{\text{H}} \sim 10^{24} \text{ cm}^{-2}$. For *XMM-Newton* and using the Bayesian hardness ratio estimation method of Park et al. (2006), we find that 50 counts will reliably differentiate a heavily obscured source with $N_{\text{H}} = 10^{24} \text{ cm}^{-2}$ from a Compton-thick source with $N_{\text{H}} = 3 \times 10^{24} \text{ cm}^{-2}$. Given the observed EPIC-pn count rate, this implies a 64 ks exposure would be required for WISE J1814+3412. Even a larger sample containing more faint and non-detections would be valuable for a stacking analysis. Assuming the obscuration is from a nuclear torus, deeper X-ray observations should detect narrow, reflected Fe $K\alpha$ fluorescent emission at rest-frame 6.4 keV (e.g., Nandra et al. 2007); a significant non-detection could point toward obscuration on larger scales than the torus. Such large-scale obscuration could also be probed by high-resolution imaging, such as far-IR observations with ALMA, and, eventually, mid-IR observations with the *James Webb Space Telescope*. Near-IR spectroscopy could also look for reddening in the AGN narrow-line region (e.g., Brand et al. 2007), which is expected to extend on scales significantly larger than those of the torus. A clearer understanding of the geometry of the obscuring region combined with an improved reckoning of the *W1W2*-dropout space density will enable us to better place this population within the context of AGNs and galaxy evolution.

We gratefully acknowledge the suggestions made by the anonymous referee, which have improved this manuscript. This work was supported under NASA Contract No. NNG08FD60C, and made use of data from the *NuSTAR* mission, a project led by the California Institute of Technology, managed by the Jet Propulsion Laboratory, and funded by the National Aeronautics and Space Administration. We thank the *NuSTAR* Operations, Software, and Calibration teams for support with the execution and analysis of these observations. This research has made use of the *NuSTAR* Data Analysis Software (NuSTARDAS) jointly developed by the ASI Science Data Center (ASDC, Italy) and the California Institute of Technology (USA). This publication makes use of data products from the *Wide-field Infrared Survey Explorer*, which is a joint project of the University of California, Los Angeles, and the Jet Propulsion Laboratory/California Institute of Technology, funded by the National Aeronautics and Space Administration. We acknowledge financial support from the Science and Technology Facilities Council (STFC) grants ST/K501979/1 (G.B.L.), ST/I001573/1 (D.M.A. and A.D.M.), and ST/J003697/1 (P.G.), and the Leverhulme Trust (D.M.A. and J.R.M.). R.J.A. was supported by Gemini-CONICYT grant number 32120009. F.E.B. acknowledges support from CONICYT-Chile (Basal-CATA PFB-06/2007, FONDECYT 1141218, and “EMBIGGEN” Anillo ACT1101) and Project IC120009 “Millennium Institute of Astrophysics (MAS)” of Iniciativa Científica Milenio del Ministerio de Economía, Fomento y Turismo. A.C. acknowledges support from ASI-INAF grant I/37/012/0-011/13. R.C.H. acknowledges support from NASA through ADAP award NNX12AE38G and the National Science Foundation through grant number 1211096. M.K. acknowledges support from Swiss National Science Foundation (NSF) grant PP00P2 138979/1.

Facilities: Keck (LRIS), *NuSTAR*, Spitzer (IRAC), XMM, WISE

REFERENCES

- Alexander, D. M., Chary, R.-R., Pope, A., et al. 2008, *ApJ*, 687, 835
 Alexander, D. M., Stern, D., Del Moro, A., et al. 2013, *ApJ*, 773, 125
 Alexandroff, R., Strauss, M. A., Greene, J. E., et al. 2013, *MNRAS*, 435, 3306
 Arévalo, P., Bauer, F. E., Puccetti, S., et al. 2014, *ApJ*, 791, 81
 Assef, R. J., Eisenhardt, P. R., Stern, D., et al. 2014, *ApJ*, submitted (arXiv:1408.1092)
 Assef, R. J., Kochanek, C. S., Brodwin, M., et al. 2008, *ApJ*, 676, 286
 Assef, R. J., Kochanek, C. S., Brodwin, M., et al. 2010, *ApJ*, 713, 970
 Assef, R. J., Stern, D., Kochanek, C. S., et al. 2013, *ApJ*, 772, 26
 Baloković, M., Comastri, A., Harrison, F. A., et al. 2014, *ApJ*, in press (arXiv:1408.5414)
 Becker, R. H., White, R. L., & Helfand, D. J. 1995, *ApJ*, 450, 559
 Brand, K., Dey, A., Desai, V., et al. 2007, *ApJ*, 663, 204
 Bridge, C., Blain, A., Borys, C., et al. 2013, *ApJ*, 769, 91
 Condon, J. J., Cotton, W. D., Greisen, E. W., et al. 1998, *AJ*, 115, 1693
 Del Moro, A., Mullaney, J. R., Alexander, D. M., et al. 2014, *ApJ*, 786, 16
 Dey, A., Soifer, B. T., Desai, V., et al. 2008, *ApJ*, 677, 943
 Donley, J. L., Koekemoer, A. M., Brusa, M., et al. 2012, *ApJ*, 748, 142
 Draper, A. R., & Ballantyne, D. R. 2010, *ApJ*, 715, 99
 Draper, A. R., & Ballantyne, D. R. 2011, *ApJ*, 729, 109
 Draper, A. R., & Ballantyne, D. R. 2012, *ApJ*, 753, 37
 Eisenhardt, P. R., Wu, J., Tsai, C., et al. 2012, *ApJ*, 755, 173
 Fiore, F., Puccetti, S., Brusa, M., et al. 2009, *ApJ*, 693, 447
 Gandhi, P., Horst, H., Smette, A., et al. 2009, *A&A*, 502, 457
 Griffith, R. L., Kirkpatrick, J. D., Eisenhardt, P., et al. 2012, *AJ*, 144, 148
 Hall, P. B., Snedden, S. A., Niederste-Ostholt, M., et al. 2004, *AJ*, 128, 534
 Harrison, F. A., Craig, W. W., Christensen, F. E., et al. 2013, *ApJ*, 770, 103
 Hasinger, G. 2008, *A&A*, 490, 905
 Hopkins, P. F., Hernquist, L., Cox, T. J., & Kereš, D. 2008, *ApJS*, 175, 356
 Hopkins, P. F., Hernquist, L., Cox, T. J., et al. 2006, *ApJS*, 163, 1
 Jansen, F., Lumb, D., Altieri, B., et al. 2001, *A&A*, 365, 1
 Jones, S. F., Blain, A. W., Stern, D., et al. 2014, *MNRAS*, 443, 146
 Just, D., Brandt, W. N., Shemmer, O., et al. 2007, *ApJ*, 665, 1004
 Kraft, R. P., Burrows, D. N., & Nousek, J. A. 1991, *ApJ*, 374, 344
 La Franca, F., Fiore, F., Comastri, A., et al. 2005, *ApJ*, 635, 864
 Lansbury, G. B., Alexander, D. M., Del Moro, A., et al. 2014, *ApJ*, 785, 17
 Lanzuisi, G., Piconcelli, E., Fiore, F., et al. 2009, *A&A*, 498, 67
 Lawrence, A. 1991, *MNRAS*, 252, 586
 Lonsdale, C. J., Smith, H. E., Rowan-Robinson, M., et al. 2003, *PASP*, 115, 897
 Luo, B., Brandt, W. N., Alexander, D. M., et al. 2013, *ApJ*, 772, 125
 Luo, B., Brandt, W. N., Alexander, D. M., et al. 2014, *ApJ*, in press (arXiv:1408.3633)
 Lutz, D., Maiolino, R., Spoon, H. W. W., & Moorwood, A. F. M. 2004, *A&A*, 418, 465
 Maiolino, R., Marconi, A., Salvati, M., et al. 2001, *A&A*, 365, 28
 Menci, N., Fontana, A., Giallongo, E., Grazian, A., & Salimbeni, S. 2006, *ApJ*, 647, 753
 Miller, B. P., Brandt, W. N., Schneider, D. P., et al. 2011, *ApJ*, 726, 20
 Murphy, K. D., & Yaqoob, T. 2009, *MNRAS*, 397, 1549
 Nandra, K., O’Neill, P. M., George, I. M., & Reeves, J. N. 2007, *MNRAS*, 382, 194
 Oke, J. B., Cohen, J. G., Carr, M., et al. 1995, *PASP*, 107, 375
 Park, T., Kashyap, V. L., Siemiginowska, A., et al. 2006, *ApJ*, 652, 610
 Proga, D., Stone, J. M., & Kallman, T. R. 2000, *ApJ*, 543, 686
 Puccetti, S., Comastri, A., Fiore, F., et al. 2014, *ApJ*, in press (arXiv:1407.3974)
 Reddy, N. A., Steidel, C. C., Fadda, D., et al. 2006, *ApJ*, 644, 792
 Schmidt, M., & Green, R. F. 1983, *ApJ*, 269, 352
 Shapley, A. E., Steidel, C. C., Pettini, M., & Adelberger, K. L. 2003, *ApJ*, 588, 65
 Simpson, C. 2005, *MNRAS*, 360, 565
 Stern, D., Assef, R. J., Benford, D. J., et al. 2012, *ApJ*, 753, 30
 Stern, D., Bunker, A. J., Spinrad, H., & Dey, A. 2000, *ApJ*, 537, 73
 Stern, D., Eisenhardt, P., Gorjian, V., et al. 2005, *ApJ*, 631, 163
 Strüder, L., Briel, U., Dennerl, K., et al. 2001, *A&A*, 365, L18
 Teng, S. H., Brandt, W. N., Harrison, F. A., et al. 2014, *ApJ*, 785, 19
 Turner, M. J. L., Abbey, A., Arnaud, M., et al. 2001, *A&A*, 365, L27
 Ueda, Y., Akiyama, M., Hasinger, G., Mijaji, T., & Watson, M. G. 2014, *ApJ*, 786, 104
 Ueda, Y., Akiyama, M., Ohta, K., & Mijaji, T. 2003, *ApJ*, 598, 886
 Weedman, D., Sargsyan, L., Leboutteiller, V., Houck, J., & Barry, D. 2012, *ApJ*, 761, 184
 Wright, E. L., Eisenhardt, P. R. M., Mainzer, A. K., et al. 2010, *AJ*, 140, 1868
 Wu, J., Tsai, C., Sayers, J., et al. 2012, *ApJ*, 756, 96